Nile Red-Based GPCR Ligands as Ultrasensitive Probes of the Local Lipid Microenvironment of the Receptor

Fabien Hanser,[a] Claire Marsol,[a,b] Christel Valencia,[b] Pascal Villa,[b] Andrey S. Klymchenko,[c] Dominique Bonnet*#[a] and Iuliia A. Karpenko*# [a]

[a] F. Hanser, Dr. C. Marsol, Dr. D. Bonnet and Dr. I. A. Karpenko, Laboratoire d'Innovation Thérapeutique, LabEx MEDALIS, UMR7200, CNRS/Université de Strasbourg, 74 route du Rhin, 67401 Illkirch-Graffenstaden, France
E-mail: i.karpenko@unistra.fr dominique.bonnet@unistra.fr

[b] C. Valencia, Dr. P. Villa, Platform of Integrative Chemical Biology of Strasbourg (PCBIS), LabEx MEDALIS, UMS 3286 CNRS/Université de Strasbourg, ESBS Pôle API, Bld Sébastien Brant, 67412 Illkirch-Graffenstaden, France.

[c] Dr. A. S. Klymchenko, Laboratoire de Bioimagerie et Pathologies, UMR 7021 CNRS/Université de Strasbourg, 74 route du Rhin, 67401 Illkirch-Graffenstaden, France.

 # These authors contributed equally to this work.

Abstract: The local lipid microenvironment of transmembrane receptors is an essential factor in GPCR signaling. However, tools are currently missing for studying endogenously expressed GPCRs in primary cells and tissues. Here we introduce fluorescent environment-sensitive GPCR ligands for probing the microenvironment of the receptor in living cells using fluorescence microscopy under no-wash conditions. We designed and synthesized antagonist ligands of the oxytocin receptor (OTR) by conjugating a high-affinity non-peptidic OTR ligand PF-3274167 to the environment-sensitive fluorescent dye Nile Red. The length of the polar PEG spacer between the pharmacophore and the fluorophore was adjusted to lower the non-specific interactions of the probe while preserving a strong fluorogenic response. We demonstrated that the new probes embed into the lipid bilayer in the vicinity of the receptor and convey the information about the local polarity and the lipid order via the wavelength-shifting emission of the Nile Red fluorophore.

Introduction

G-protein coupled receptors (GPCRs) are a superfamily of transmembrane receptor proteins that are ubiquitously expressed in the human body and widely involved in human physiology and pathophysiology. GPCRs represent the most intensively studied targets for small-molecule therapeutics. For instance, more than 470 (> 30%) of currently marketed drugs act on over a hundred of unique GPCRs, with hundreds of prospective drugs being in preclinical development and clinical trials.[1–4] The field of GPCR research had been boosted by the recent breakthrough in the structural biology of transmembrane receptors, which revealed the three-dimensional architecture and conformational dynamics of isolated receptors, receptor−ligand and receptor−transducer protein complexes at an unprecedented atomic-level resolution. These findings gave numerous structural insights into the selectivity of ligand recognition and mechanisms of the signal transduction, facilitating further biochemical and pharmacological exploration of this class of drug targets.[5–7] Although these advances have opened new avenues for the rational development of GPCR-targeting drugs, we still have only a dim understanding of the GPCR activation and signal transduction in the complex cellular context. GPCRs are embedded into highly heterogeneous and dynamic cellular membranes, where lipid organization and the presence of lipid nanodomains[8,9] can modulate the functioning of the receptor. To

fill the gap between the growing body of structural information obtained on purified receptors *ex vivo*[10] and understanding their functioning and the heterogeneity of signaling in living cells, a multitude of chemical, pharmacological and optical tools has been developed.[11–15] Fluorescence-based methods are of particular interest for studying GPCR in their native environment because of their high sensitivity, high spatial and temporal resolution and possibility to apply them in intact living cells and tissues.[16,17] Besides that, the key advantage of fluorescence sensing is the possibility to directly and site-specifically probe dynamic molecular interactions using environment-sensitive small-molecule fluorescent reporters.[18,19]

Local alterations of the lipid microenvironment, such as the presence of highly organized lipid nanodomains, known as lipid rafts, can affect the conformation equilibrium of the transmembrane receptor, its affinity to ligands and its protein-protein interactions.[20–25] Therefore, studying the lipid microenvironment of receptors is of fundamental importance for understanding and modulating GPCR signaling.[26] However, the progress has been hampered by the lack of reliable experimental methods and by the multiple controversies related to the lipid raft hypothesis.[27] Environment-sensitive probes, such as LAURDAN,[28] di-4-ANEPPDHQ,[29] Nile Red (NR) derivatives,[30,31] could be used to address the lipid order in biomembranes through shifts in the emission color.[32] However, these probes report the average lipid order of the bulk of cell membrane and are not suitable for probing specifically the receptor microenvironment. One work addressed probing of the local receptor microenvironment within the Förster radius by using time-resolved FRET from a GLP-1 receptor labeled with a long-life luminescent terbium cryptate to NR-based probe NR12S.[33] However, studying the local lipid microenvironment of untagged GPCRs in intact living cells and tissues remains a formidable challenge. In our previous works, we synthesized optically-responsive chemical probes targeting the oxytocin receptor (OTR), a class A GPCR. In our design, a peptidic agonist of the receptor was covalently tethered to the NR fluorophore.[34] The resulting conjugate delivered the fluorescent probe directly into the lipid bilayer in the vicinity of the receptor. Being non-fluorescent in water, the conjugate displayed a strong enhancement of fluorescence upon binding to the receptor, enabling qualitative and quantitative detection of the receptor under wash-free conditions. Although the solvatochromic properties of Nile Red have been successfully used for probing the polarity and molecular organization of biological membranes,[30,31,35,36] the utility of our first-generation OTR-targeting fluorescent probes for studying the lipid microenvironment of the native receptors was limited because of their agonism. Binding of the probes to the OTR triggered fast cellular response resulting in the rapid internalization of the receptor which is usually associated with the dramatic changes of lipid composition of the receptor within the endosomal compartment. In the present work, we address these limitations and report a new generation of GPCR-targeting fluorescent probes. To overcome the problem of receptor internalization, we designed, synthesized and characterized a series of antagonist-based conjugate delivering the environment-sensitive fluorogenic Nile Red-based probe into the vicinity of the OTR. We used a combination of steady-state fluorescence spectroscopy and ratiometric confocal fluorescence microscopy to demonstrate the ability of the new probes to embed into the lipid bilayer in the vicinity of the receptor in living cells and to transmit the information about the properties of the local lipid microenvironment via the color-shifting emission of the NR fluorophore.
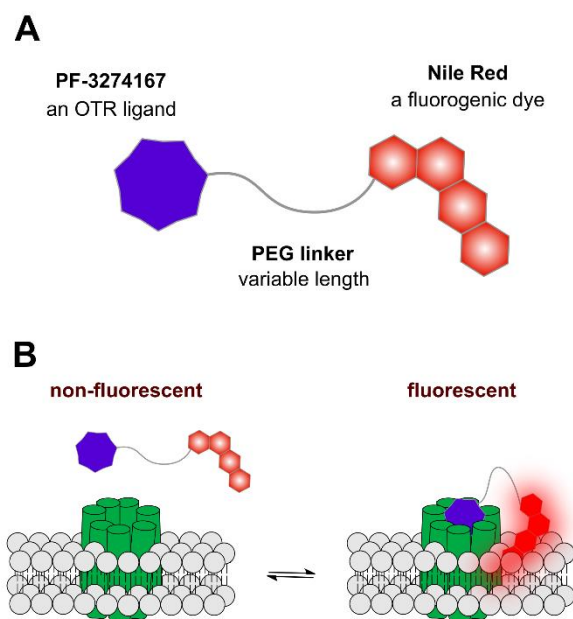
Figure 1. The design (A) and the working principle (B) of the fluorogenic non-peptidic OTR ligands.

Results and Discussion

Design and Synthesis. To design antagonist-based environment-sensitive conjugates targeting the OTR we used the approach that had been validated on peptidic OTR agonists.[34] Solvatochromic fluorogenic NR dye was covalently tethered to a non-peptidic antagonist of the OTR via a flexible linker of variable length (Figure 1A). NR-based carboxylic acid NR-COOH (**4**, Scheme 1) and the desmethyl precursor of the OTR-selective antagonist PF-3274167[37,38] were chosen as the key structural blocks to be conjugated through a flexible polyethylenglycol (PEG)-based tethers of variable length. Four PEG linkers composed of 4 – 20 ethylenic moieties were selected and tested to decrease the off-target binding of the probes and to finely tune the specificity of the probe and its fluorogenic response upon homogenous wash-free imaging condition (Figure 1B). First, we revised the synthesis of NR-COOH **4** (Scheme 1). The procedure reported in the literature starts from the conversion of commercially available 3-diethylaminophenol **1** into nitrosophenol **2**, which is then engaged into an intermolecular oxidative cyclization with 1,6-dihydroxynaphthalene to give the phenol derivative of Nile Red **3**. According to the original protocols,[39,40] nitrosophenol **2** was purified by recrystallization from ethanol/diethyl ether mixture and then refluxed in DMF with 1,6-dihydroxynaphthalene to give the desired compound **3** in moderate yield of 42% over two steps.
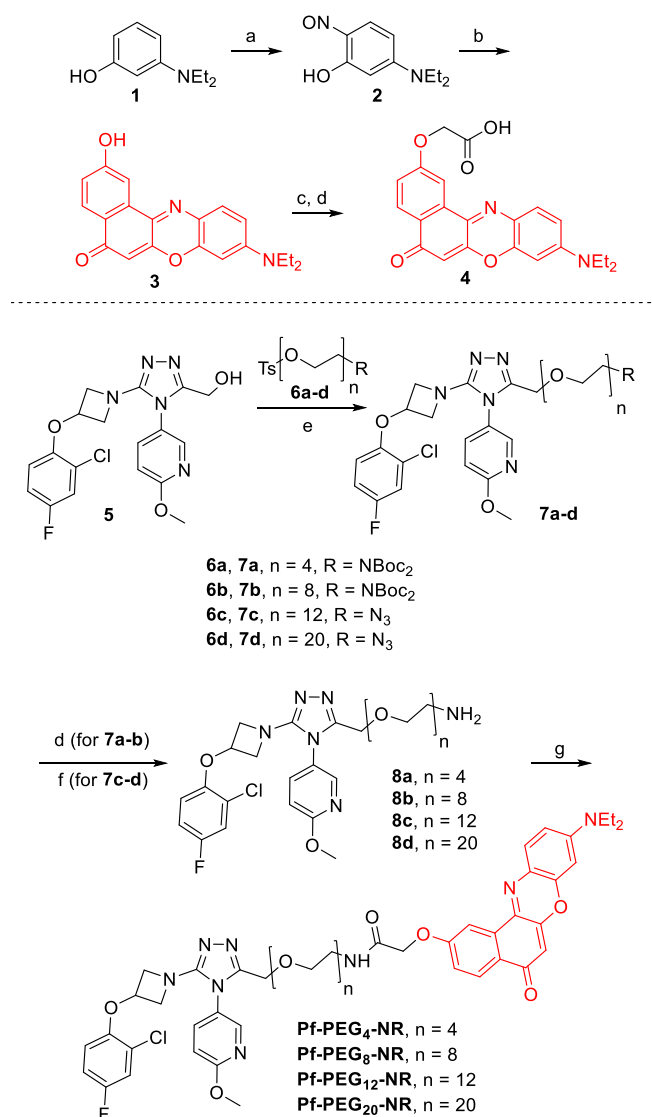
Scheme 1. Synthesis of the non-peptidic fluorescent OTR ligands. a) NaNO$_2$, HCl, H$_2$O, 0 °C, 2.5 h. b) 1,6-Dihydroxynaphthalene, DMF, 110 °C, 45 min. c) *tert*-Butyl chloroacetate, K$_2$CO$_3$, acetone, reflux, 6.5 h. d) Trifluoroacetic acid, DCM, 25 °C, 0.5–3.5 h. e) KOH, DMF, 0–45 °C, 2.5–67 h. f) Triphenylphosphine polymer-bound, THF, reflux then H$_2$O, reflux, 5–7 h. g) **4**, PyBOP, DIPEA, DMF, 25 °C, 0.5–25 h..

However, in our hands the recrystallization of nitrosophenol **3** was not robustly reproducible. To make things worse, nitrosophenol was found to decompose upon boiling in DMF, resulting in highly variable and significantly lower yields of Nile Red derivative **3** (27% at best). We improved the synthetic protocol by omitting the problematic crystallization step. We found that better yields of **3** were obtained when the crude nitrosophenol **2** was isolated by evaporation of the acidic reaction mixture and engaged into the cyclization without further purification. The intermolecular cyclization was carried out with 2 equiv. of nitrosophenol **2** in DMF at 110°C for 45 min. Following the proposed protocol, the phenol derivative of Nile Red **3** was obtained in 44% yield over two steps. The protocol was robustly reproducible on 0.45 - 3 mmol scale. Phenol **3** was then alkylated with *tert*-butyl chloroacetate[41] and then *tert*-butyl protecting group was removed by the treatment with trifluoroacetic acid to afford NR-COOH **4** in 84% yield over two steps (Scheme 1).

The synthesis of the desmethyl precursor of PF-3274167 **5** and its two pegylated derivatives **8a** and **8b** bearing PEG$_4$ and PEG$_8$ chains (Scheme 1) was performed following our previously established protocols.[38] Regarding PEG$_{12}$ and PEG$_{20}$ derivatives **8c** and **8d**, we found it more convenient to synthesize these amines by reducing the corresponding azides. To achieve this, we first alkylated the desmethyl precursor of PF-3274167 **5** with azido-tosylates **6c** and **6d** in the presence of KOH in DMF affording pegylated triazoles **7c** and **7d** in 92% and 72% yield, respectively. Next, **7c** and **7d** were converted into amines **8c** and **8d** using the Staudinger reduction in the presence of polymer-bound triphenylphosphine. Finally, coupling of amines **8a-d** to NR-COOH led to the formation of the desired OTR non-peptidic ligands Pf-PEG$_4$-NR, Pf-PEG$_8$-NR, Pf-PEG$_{12}$-NR and Pf-PEG$_{20}$-NR.

Spectroscopic Characterization. The fluorescence properties of the Nile Red derivatives were first studies in a series of solvents of different polarity. Steady-state fluorescence spectra of the OTR ligands (Figure 2A) revealed that the strong solvatochromic and fluorogenic character of Nile Red was retained upon conjugation of NR-COOH to the OTR ligand via the PEG linkers. All the four OTR ligands were highly fluorescent in apolar solvents such as 1,4-dioxane with the emission maxima of about 585 nm (Table 1). Due to the positive solvatochromism of Nile Red, the emission maxima in water bathochromically shifted to 660 nm, and the fluorescence quantum yields gradually decreased with the increasing polarity of the solvent.

Table 1. Fluorescence properties of the NR conjugates.

| Solvent | λ_{max}, nm | | QY[c] | | | |
	abs[a]	fluor[b]	Pf-PEG$_4$-NR	Pf-PEG$_8$-NR	Pf-PEG$_{12}$-NR	Pf-PEG$_{20}$-NR
1,4-Dioxane	521	584	65	65	67	68
Acetone	534	612	65	64	65	66
Acetonitrile	538	619	62	60	63	65
Ethanol	551	634	48	48	51	52
Methanol	556	639	37	38	39	41
Water	601	661	7	10	11	11

[a] Position of the absorption maximum. Similar values (+/- 2 nm) were observed for all the four conjugates. [b] Position of the emission maximum. Similar values (+/- 2 nm) were observed for all the four conjugates. [c] Fluorescence quantum yield.

An important parameter for cellular studies upon wash-free conditions is the fluorescence turn-on ratio, a quantitative measure of the fluorogenic properties of the probes. Here we define it as the ratio of the fluorescence intensity at 620 nm in an apolar solvent (1,4-dioxane) to that in water. All the four NR conjugates demonstrated excellent fluorogenic properties with relative turn-on ratios ranging from 18- to 35-fold (Figure 2B).
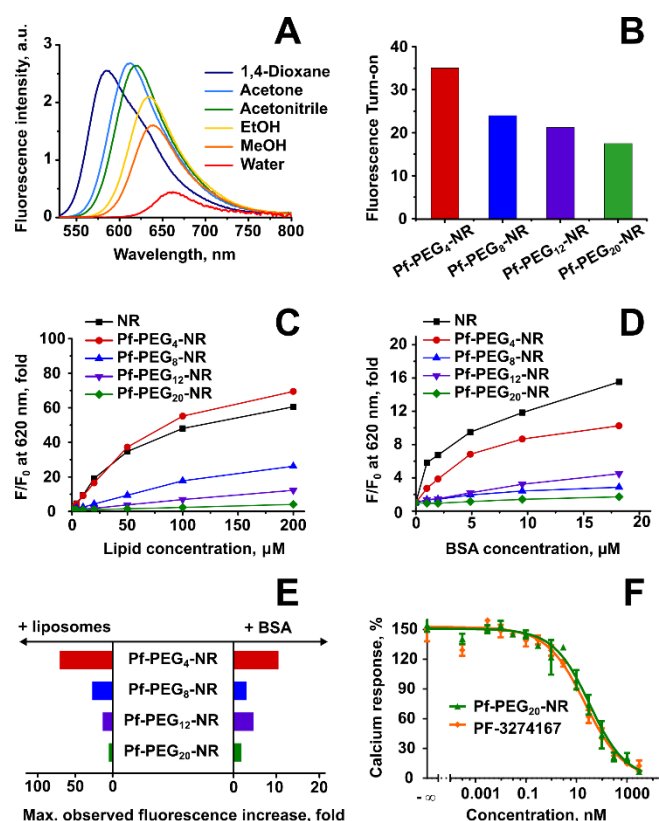

Figure 2. Fluorescence and pharmacological properties of the OTR ligands. (A) Fluorescence spectra of Pf-PEG$_4$-NR in different solvents. Fluorescence intensity is normalized to the absorbance at 520 nm (B) Fluorogenic properties of the OTR fluorescent ligands. The relative fluorescence turn-on was calculated as a ratio of the fluorescence intensity at 620 nm in 1,4-dioxane (normalized to the absorbance at 520 nm) to that in water (normalized to the absorbance at 520 nm). (C) Evaluation of non-specific interactions of the OTR ligands and Nile Red (NR) with DOPC/cholesterol (2:1) liposomes: fluorescence intensity increase at 620 nm (F/F0) as a function of liposomes concentration in PBS. (D) Evaluation of non-specific interactions of the OTR ligands and Nile Red (NR) with BSA: fluorescence intensity increase at 620 nm (F/F0) as a function of BSA concentration in PBS. (E) Maximal observed fluorescence increase due to non-specific interactions of the OTR ligands with liposomes and BSA. (F) Dose-response curves for OTR antagonists PF-3274167 and Pf-PEG$_{20}$-NR. Data from two independent experiments performed in duplicate. Values are means ± SEM.

Evaluation of Non-Specific Interactions. In the development of fluorescent probes for live-cell studies of membrane receptors it is crucial to carefully evaluate the non-specific interactions of the probes with cellular membranes and serum proteins. To address this issue, we used 1,2-dioleoyl-sn-glycero-3-phosphocholine (DOPC) / cholesterol (2:1) large unilamellar vesicles (LUVs) as a model of cell membranes and BSA to evaluate the binding to plasma proteins. Nile Red is known for its strong non-specific binding to lipid membranes,[42] lipid droplets[43] and hydrophobic protein pockets.[44–46] In our

hands, fluorescence of Nile Red (Figures 2C and 2D, black line) did gradually increase upon addition of liposomes or BSA to its aqueous solution. The NR conjugates were evaluated under the same conditions. As we expected based on our previous work with the OTR agonists, the increase of the length of the polar PEG spacer resulted in a gradual decrease of the non-specific interactions (Figure 2E). For instance, Pf-PEG$_4$-NR bound the liposomes with similar affinity to Nile Red. Its interaction with BSA was less pronounced comparing to unmodified Nile Red but still significant, making this probe poorly compatible with the live-cells imaging conditions. Although Pf-PEG$_8$-NR and Pf-PEG$_{12}$-NR did not display significant binding to BSA, they were still strongly interacting with model membranes. Finally, the non-specific binding to lipid membranes and BSA became almost negligible for Pf-PEG$_{20}$-NR, making this ligand the most promising for cellular studies of the OTR.

Functional Characterization. In order to verify whether the introduction of a long PEG$_{20}$ spacer influenced the functional activity of the PF-3274167 pharmacophore, we measured its effect on the calcium response in HEK 293 cells stably overexpressing the OTR (HEK-OTR cells). Both the unmodified PF-3274167 and Pf-PEG$_{20}$-NR fully inhibited the oxytocin-induced calcium accumulation in a dose-dependent manner with similar IC$_{50}$ of 15 ± 3 nM and 30 ± 3 nM, respectively, highlighting the antagonist character of both ligands (Figure 2F). Thus, the introduction of a cumbersome PEG$_{20}$ spacer capped with the aromatic fluorophore has a low impact on the functional activity of the ligand which retained its antagonist character.

Wash-Free Imaging of the OTR in Living Cells. Next, the confocal microscopy study on living HEK-OTR cells was performed in order to evaluate the ability of the developed probes to detect the receptor under wash-free conditions. We were pleased to find that Pf-PEG$_{20}$-NR, the conjugate having the most favorable combination of properties in the non-specific binding assay, showed exclusive localization on the plasma membrane. Importantly, the OTR retained on the cell membrane with no detectable ligand-induced internalization, due to the antagonist character of PF-3274167 (Figure 3). A competition assay was then used to demonstrate the specificity of the probe towards the OTR. Indeed, upon addition of a large excess of a non-fluorescent OTR-binding competitor carbetocin (CBT), the plasma membrane signal disappeared, indicating that Pf-PEG$_{20}$-NR binds to the cell reversibly in a receptor-specific manner. We also confirmed by confocal microscopy that the ligands with the PEG chains of 4, 8 and 12 units exhibited a strong non-specific binding, as one would have expected from the *in vitro* non-specific binding assay (Figure 2C-E). Their fluorescence was not influenced by the addition of the non-fluorescent competitor and, moreover, these ligands rapidly crossed the plasma membrane and stained intracellular structures.
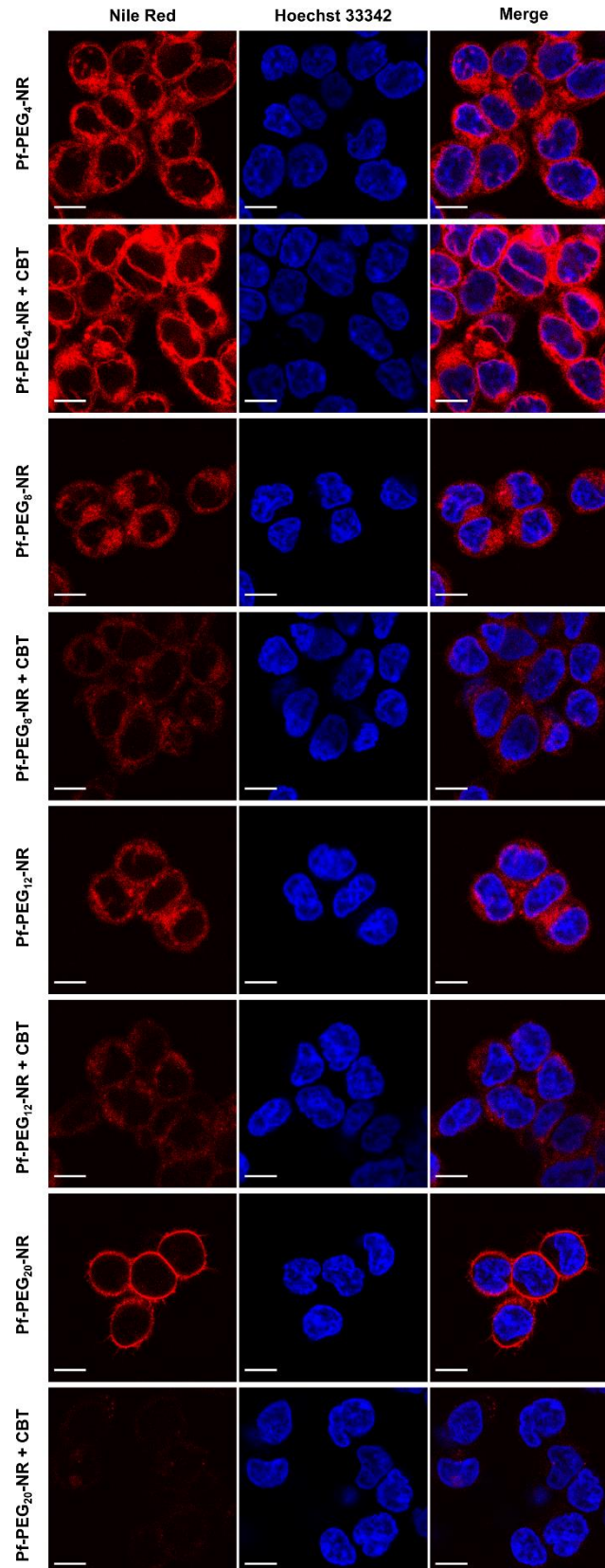
Figure 3. Confocal microscopy of the fluorogenic OTR ligands in living HEK293 cells overexpressing the OTR under no-wash conditions. Non-specific binding is evaluated in the presence of a 200-fold excess of the non-fluorescent OTR ligand carbetocin (CBT). Concentrations: OTR ligands 10 nM, CBT 2 µM. The cells were incubated with fluorescent ligands for 20 min at 37 °C prior to the imaging. Fluorescence of Nile Red (570 – 630 nm) is shown in red, nuclei stained with Hoechst 33342 are shown in blue. Scale bars, 10 µm.

Ratiometric Confocal Microscopy Studies of Local Probe Microenvironment. To demonstrate the utility of the fluorogenic NR-based ligands for selective probing of the receptor microenvironment, ratiometric confocal microscopy experiments were performed under wash-free conditions on living HEK-OTR cells. We used a ratiometry-based fluorescence sensing, which is insensitive to the concentration of the ligand and the expression level of the receptor, facilitating quantitative analysis of fluorescence data.[19] Upon excitation with the 488 nm laser, the emitted light was collected separately in two channels, referred here as the "green" (500-600 nm) and the "red" (600-700 nm) channels. Taking into account the positive fluorescence solvatochromism of Nile Red derivatives, one could expect that a stronger fluorescence in the "red" channel indicates a more polar (or less hydrophobic) microenvironment. Accordingly, a stronger fluorescence in the "green" channel indicates less polar (or more hydrophobic) microenvironment of the fluorophore (Figure 4A). In other words, the relative "red-to-green" ratio (RTG) can be used as a simple quantitative measure of the polarity of the microenvironment of the probe.

The observed RTG values differed dramatically for Pf-PEG$_{20}$-NR and the other OTR ligands with shorter linker length in the cellular context (Figure 4B-E). In living cells, the fluorophore of Pf-PEG$_{20}$-NR was surrounded by a strongly apolar microenvironment with a mean RTG value of 0.90 ± 0.04. For comparison, the observed mean RTG value of the membrane probe NR12S[30] (Figure 5A) localized in the outer leaflet of the plasma membrane was 0.73 ± 0.01. In contrast, the fluorescence of the Nile Red derivatives with shorter PEG linkers was shifted to the red with mean RTG values above 1.5. These data confirmed the conclusion drawn from the confocal microscopy images (Figure 3) about the undesired penetration of the probes with PEG lengths of 4, 8 and 12 inside the cell. It also suggested that the mentioned probes reside within intracellular membrane compartment of different composition compared to the outer leaflet of the cell membrane. The observed higher RTG values inside the cells for the probes with short PEG linkers reflect higher polarity of the intracellular membranes compared to the plasma membranes, previously reported by cell permeable solvatochromic probes.[47] On the other hand, Pf-PEG$_{20}$-NR does not penetrate inside the cell and is localized within a rather apolar environment, likely within the lipid bilayer in the vicinity of the receptor.
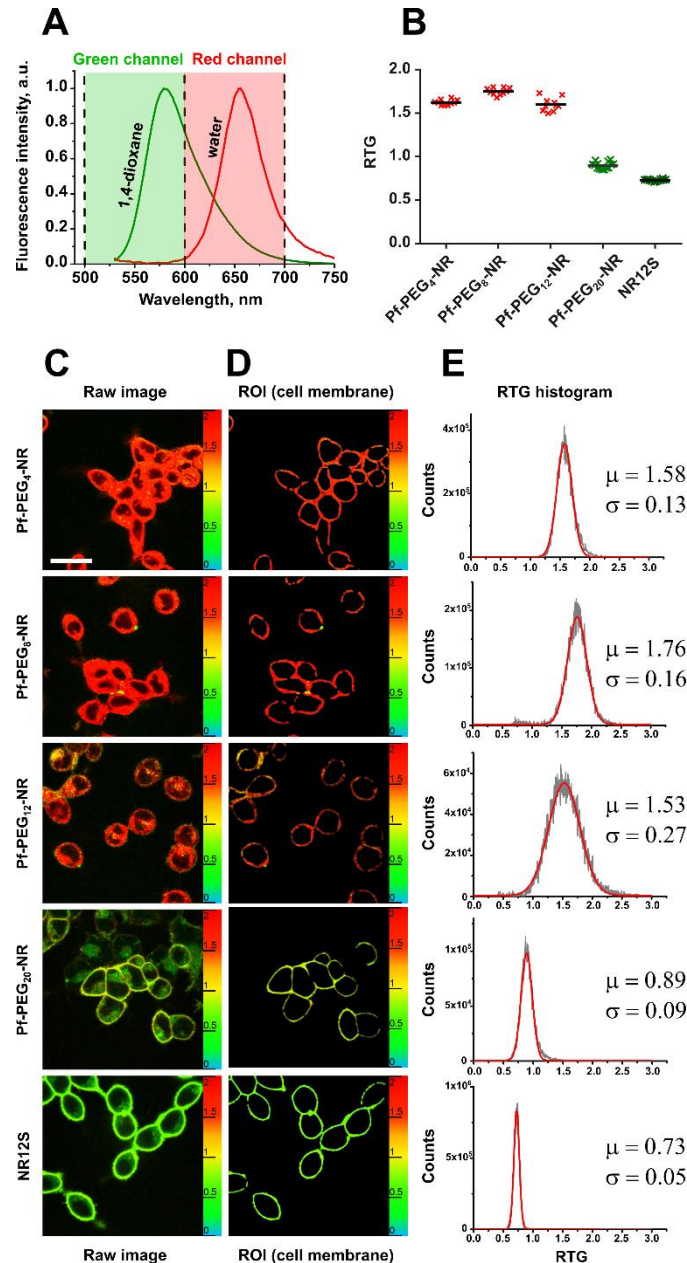
Figure 4. Ratiometric confocal microscopy imaging with NR-based probes. (A) Uncorrected normalized fluorescence spectra of Pf-PEG$_4$-NR in 1,4-dioxane and water with the indication of the green and the red channels used for the calculation of the RTG ratio. (B) Comparison of mean RTG values resulted from the cellular staining for different probes. Data from two biological replicates, five to seven images per condition were analyzed. (C) Imaging of living HEK293 cells overexpressing the OTR with the NR conjugates and NR12S[30] (*vide infra*) under no-wash conditions. The pseudocolor scale indicates RTG values of the Nile Red fluorescence. Scale bar, 30 µm. (D) ROI used for quantification. (E) Frequencies (grey) and adjusted normal distributions (red) of RTG values for the ROI presented in (D).

To further address the question of the localization of the fluorophore in Pf-PEG$_{20}$-NR bound to the OTR, we compared it with the previously reported specific peptidic OTR ligand CBT-NR[34] lacking a flexible spacer between the fluorophore and the pharmacophore (Figure 5A). Although the structure of OTR bound to a peptidic ligand has not been solved yet, the recently published crystal structure of the OTR bound to a non-peptidic antagonist provides insights on the structure of the orthosteric binding pocket

of the receptor. The study demonstrated that the OTR possesses an enlarged orthosteric binding site, situated at the extracellular part of the receptor and comprised of a polar solvent-exposed interaction surface and a hydrophobic crevice.[48] In such case, it is highly unlikely that the fluorophore in CBT-NR–OTR complex could be deeply embedded into the cell membrane. Most probably, the fluorophore in CBT-NR bound to the OTR resides within its large ligand-binding pocket or an allosteric binding site. We obtained a mean RTG value of 1.13 ± 0.02 for CBT-NR bound to the OTR (Figure 5B), which indicates that the fluorophore resides within a more polar environment comparing to that of the bulk cellular membrane reported by NR12S (mean RTG value of 0.73 ± 0.01). This result is in line with the hypothesis that the fluorophore in CBT-NR is not embedded into the membrane. For the non-peptidic OTR ligand Pf-PEG$_{20}$-NR, its microenvironment characterized by a mean RTG value of 0.90 ± 0.04, was different from that of the 'linkerless' OTR ligand CBT-NR. The mean RTG value of Pf-PEG$_{20}$-NR also appeared to be different from the membrane-averaged RTG value measured with the membrane probe NR12S (0.73 ± 0.01), indicating that Pf-PEG$_{20}$-NR could uniquely probe the local lipid bilayer surrounding the transmembrane receptor.
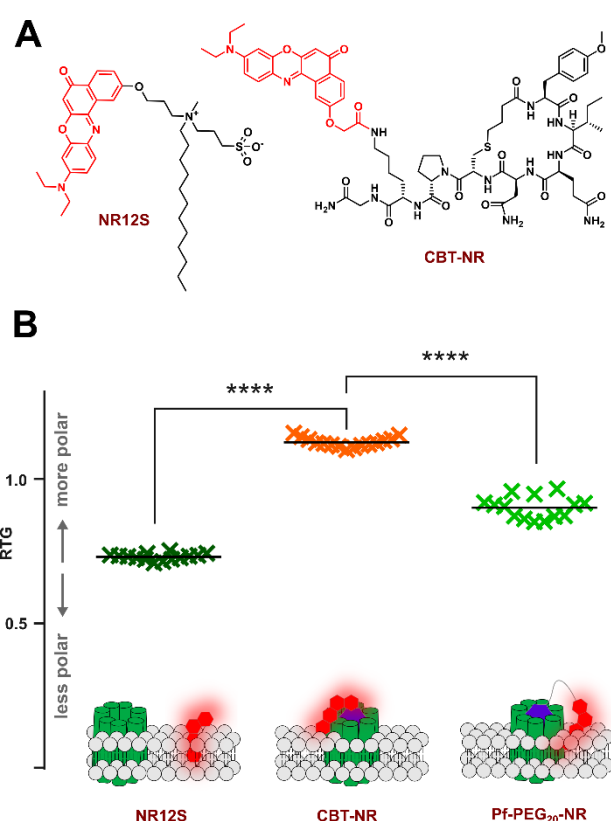

Figure 5. Evaluation of the polarity of the local microenvironment of the OTR. (A) Chemical structure of the membrane probe NR12S[30] and the peptidic OTR ligand CBT-NR[34]. (B) Comparison of mean RTG values resulted from the cellular staining for different probes. NR12S reports the properties of the bulk membrane, CBT-NR reports from a receptor ligand-binding pocket or an allosteric binding site, Pf-PEG20-NR reports from the lipid bilayer in the vicinity of the receptor. Data from two biological replicates, seven images per condition were analyzed. Statistics: one-way ANOVA with Tukey's multiple comparison test (confidence interval 99%, adjusted p values: **** < 0.0001).

If the suggestion that Pf-PEG$_{20}$-NR resided in the lipid bilayer in the vicinity of the receptor was correct, the probe should report changes in the lipid composition of the cell membrane. Klymchenko et al.[30] showed that the membrane probe NR12S displayed a red shift of fluorescence spectrum upon treatment of living U87MG cells with methyl-β-cyclodextrin (MβCD). One of the known effects of MβCD treatment is cholesterol depletion, which would decrease the number and size of the cholesterol-rich ordered (L$_O$) microdomains in the plasma membrane.[49] We performed MβCD treatment in our cell line (HEK293) stably overexpressing the OTR in presence of the NR-based probes. The emission of NR12S shifted slightly to the red upon MβCD treatment as follows from the increase of its mean RTG value from 0.73 ± 0.01 to 0.79 ± 0.02 (Figure 6). Under the same condition, the receptor-bound probe Pf-PEG$_{20}$-NR displayed a similar trend by increasing its mean RTG value from 0.90 ± 0.04 to 0.98 ± 0.08. The unidirectional shift of the mean RTG for the both probes supports out suggestion that the fluorophore of the Pf-PEG$_{20}$-NR probe reaches the membrane and reports the changes of local lipid environment of the receptor.
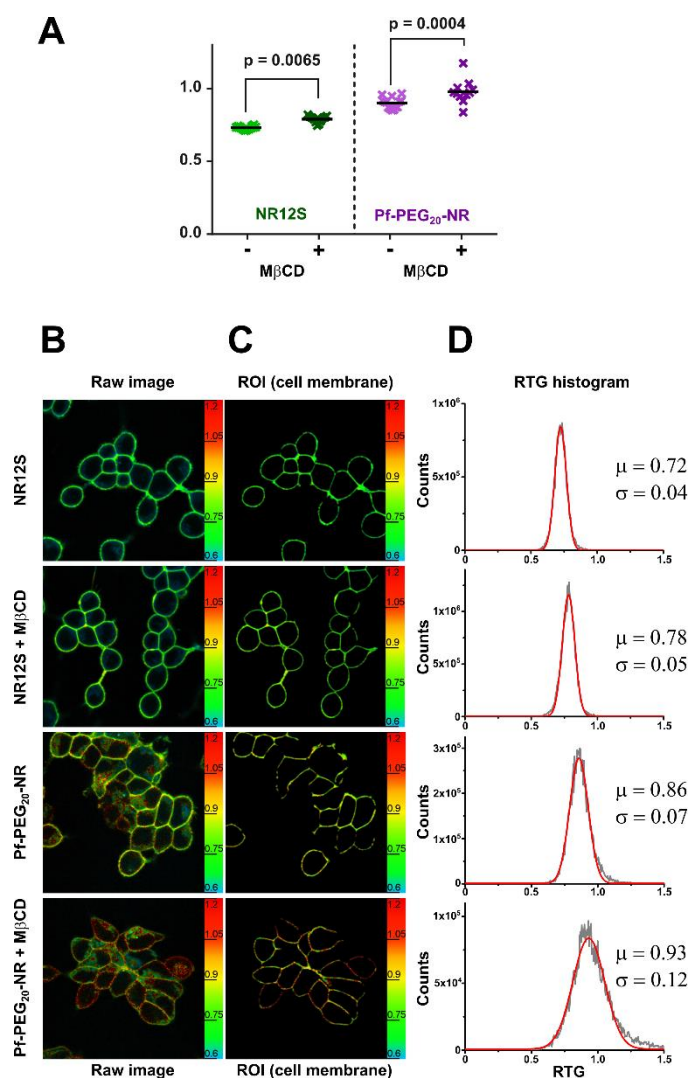

Figure 6. Influence of the MβCD treatment on the local microenvironment of the OTR. (A) Comparison of mean RTG values resulted from the cellular staining with Pf-PEG$_{20}$-NR and NR12S before and after the MβCD treatment. Data from two biological replicates, seven images per condition were analyzed. Statistics: one-way ANOVA with Tukey's multiple comparison test (confidence interval 99%). (B) Imaging of living HEK293

cells overexpressing the OTR stained Pf-PEG$_{20}$-NR and NR12S under no-wash conditions before and after the MβCD treatment. The pseudocolor scale indicates RTG values of the Nile Red fluorescence. Scale bar, 30 µm. (C) ROI used for quantification. (D) Frequencies (grey) and adjusted normal distributions (red) of RTG values for the ROI presented in (C).

Conclusions

In this work, we developed first environment-sensitive antagonist probes for the oxytocin GPCR by covalently tethering the Nile Red fluorophore to a non-peptidic OTR antagonist. Our best probe Pf-PEG$_{20}$-NR featured a combination of excellent fluorogenicity, strong positive solvatochromism and negligible non-specific binding to lipid membranes and serum proteins. It enabled fluorescence imaging of the OTR in cultured cells under wash-free conditions with negligible background fluorescence. The new conjugate also enabled direct fluorescence ratiometric probing of the local plasma membrane microenvironment in the proximity to the transmembrane receptor. To date, very few methods are available for studying lipid heterogeneity of the cell membrane in space and time. None of these methods has been used for the analysis of lipid bilayer in the vicinity of an unmodified G protein-coupled receptor. In this context, Pf-PEG$_{20}$-NR represents the first fluorescent GPCR ligand able to probe the microenvironment of the unmodified receptor. The probe design presented in this work could be easily expanded for studies of other membrane receptors.

Experimental Section

Materials and Methods

Reagents were obtained from commercial sources and used without any further purification. Compounds **5**, **6a**, **6b**, **7a**, **7b**, **8a** and **8b** were synthesized following the previously published protocols.[38] Compound **6c** was synthesized according to Zhang, et al.[50] Thin-layer chromatography was performed on Merck silica gel 60F254 plates. VWR silica gel (40-63 µm) was used for chromatography columns. Semi-preparative reverse-phase HPLC purifications were performed on a Waters SunFire C18 OBD Prep column (5 µm, 19 × 150 mm) on a Gilson PLC2020 system. Reverse-phase flash purifications were performed on prepacked Puriflash C18 columns from Interchim on a Gilson PLC2020 system. Analytical reverse-phase HPLC were performed on an Ascentis Express C18 column (2.7 µm, 4.6 mm × 75 mm) on an Agilent Technologies 1200 series HPLC system using a linear gradient (5% to 100% v/v in 7.3 min, flow rate of 1.6 mL.min^{-1}) of solvent B (0.1% v/v TFA in ACN) in solvent A (0.1% v/v TFA in H$_2$O). ^{1}H NMR spectra were recorded at 400 MHz and 500 MHz and ^{13}C NMR spectra were recorded at 101 MHz and 126 MHz, on a Bruker Advance spectrometer. Chemical shifts are reported in parts per million (ppm), coupling constants (J) are reported in hertz (Hz). Signals are described as s (singlet), d (doublet), t (triplet), q (quadruplet), p (pentuplet) and m (multiplet). Low resolution mass spectra (LRMS) and high resolution mass spectra (HRMS) were obtained on an Agilent Technologie 6520 Accurare-Mass Q.Tof LC/MS apparatus equipped with a Zorbax SB C$_{18}$ column (1.8 µm, 2.1 × 50 mm) using electrospray ionization (ESI) and a time-of-flight analyzer (TOF). Absorption and fluorescence measurement were performed in 114F-QS 10 mm quartz fluorescence cuvettes (Hellma Analytics). Absorption spectra were recorded on a Cary 4000-HP spectrophotometer (Varian) and fluorescence spectra on a FluoroMax 4 (Jobin Yvon, Horiba) spectrofluorometer equipped with a

thermostated cuvette holder at 20 °C. The solvents used were either of spectroscopy or HPLC grade. Fluorescence confocal microscopy experiments were performed on a Leica TCS SPE-II microscope with an HXC PL APO 63x/1.40 OIL CS objective.

Synthesis

5-(diethylamino)-2-nitrosophenol (2). To a solution of **1** (1.00 g, 5.87 mmol, 1 eq.) in a mixture of water (6 mL) and concentrated HCl (6 mL, 70.5 mmol, 12 eq.) at iced water temperature was dropwise added a solution of $NaNO_2$ (418 mg, 5.87 mmol, 1 eq.) in water (4 mL) over a period of 30 min. The mixture was stirred at iced water temperature for 2 h and then concentrated under vacuum to afford a brown solid (1.14 g). This unstable product was directly used for the next step. HPLC t_R = 2.22 min (> 95% purity [220.8 nm]). ^{1}H NMR (400 MHz, $CDCl_3$) δ 7.31 (d, J = 9.9 Hz, 1H), 6.53 (dd, J = 9.9, 2.5 Hz, 1H), 5.66 (d, J = 2.6 Hz, 1H), 3.48 (q, J = 7.0 Hz, 4H), 1.26 (t, J = 7.2 Hz, 6H). ^{13}C NMR (101 MHz, $CDCl_3$) δ 169.36, 157.23, 149.68, 135.57, 113.69, 96.12, 46.07, 13.00.

9-(diethylamino)-2-hydroxy-5H-benzo[a]phenoxazin-5-one (3). A solution of naphthalene-1,6-diol (73.0 mg, 0.45 mmol, 1 eq.) in anhydrous DMF (4 mL) was added to a solution of **2** (175 mg, 0.90 mmol, 2 eq.) in anhydrous DMF (1 mL). The mixture was stirred at 110 °C for 45 min. DMF was removed under reduced pressure and the crude product was purified by reverse-phase flash chromatography using a linear gradient of 15-70% ACN (0.1%TFA) in H_2O (0.1% TFA) in 30 min to afford after lyophilization a dark purple solid (66.5 mg, 44%). HPLC t_R = 4.57 min (> 95% purity [220.8 nm]). ^{1}H NMR (500 MHz, DMSO-d_6) δ 10.40 (s, 1H), 7.96 (d, J = 8.6 Hz, 1H), 7.87 (d, J = 2.5 Hz, 1H), 7.56 (d, J = 9.0 Hz, 1H), 7.08 (dd, J = 8.6, 2.5 Hz, 1H), 6.78 (dd, J = 9.1, 2.7 Hz, 1H), 6.62 (d, J = 2. 7 Hz, 1H), 6.14 (s, 1H), 3.48 (q, J = 7.1 Hz, 4H), 1.15 (t, J = 7.0 Hz, 6H). ^{13}C NMR (126 MHz, DMSO) δ 181.37, 159.78, 151.56, 150.71, 144.95, 138.59, 134.87, 132.01, 128.40, 125.16, 123.11, 118.34, 110.01, 107.47, 105.80, 95.33, 45.28, 12.98.

2-((9-(diethylamino)-5-oxo-5H-benzo[a]phenoxazin-2-yl)oxy)acetic acid (4). To a solution of **3** (537 mg, 1.60 mmol, 1 eq.) and K_2CO_3 (1.32 g, 9.58 mmol, 6 eq.) in acetone (16 mL) was added *tert*-butyl chloroacetate (0.7 mL, 4.79 mmol, 3 eq.). The mixture was stirred under reflux for 6.5 h. The solvent was evaporated under reduced pressure and the residue was dissolved in ethyl acetate (50 mL), washed with water and brine, dried over anhydrous Na_2SO_4 and concentrated under reduced pressure. The obtained residue was dissolved in DCM (9 mL) and TFA (6 mL) was added. The mixture was stirred at 25 °C for 1.5 h. After evaporation of the volatiles under reduced pressure, ethyl acetate (50 mL) was added and the organic layer was washed with water and brine, dried over anhydrous Na_2SO_4 and concentrated under reduced pressure. The crude product was purified by reverse-phase flash chromatography using a linear gradient of 30-80% ACN (0.1% TFA) in H_2O (0.1% TFA) in 30 min to afford after lyophilization a dark purple solid (721 mg, 84%). HPLC t_R = 4.57 min (> 95% purity [220.8 nm]). ^{1}H NMR (DMSO-d_6) δ 8.01 (d, J = 8.7, 1H), 7.84 (d, J = 2.7 Hz, 1H), 7.53 (d, J = 9.1 Hz, 1H), 7.24 (dd, J = 8.7, 2.7 Hz, 1H), 6.79 - 6.72 (m, 1H), 6.57 (d, J = 2.6 Hz, 1H), 6.14 (s, 1H), 4.87 (s, 2H), 3.46 (m, 4H), 1.15 (t, J = 7.0 Hz, 6H). ^{13}C NMR (DMSO) δ 181.12, 169.74, 160.26, 151.68, 150.86, 146.42, 137.97, 133.40, 130.91, 127.19, 125.23, 124.00, 117.80, 110.14, 106.51, 103.98, 95.94, 64.74, 44.43, 12.43.

59-azido-3,6,9,12,15,18,21,24,27,30,33,36,39,42,45,48,51,54,57-nonadecaoxanonapentacontyl 4-methylbenzenesulfonate (6d). To a solution of N3-PEG(20)-OH (50.0 mg, 54.1 µmol, 1 eq.) in anhydrous DCM (1 mL) were added 4-methylbenzenesulfonyl chloride (21 mg, 108 µmol, 2 eq.) and

KOH (18.2 mg, 325 µmol, 6 eq.). The mixture was stirred at iced water temperature for 1 h then at room temperature for 3 days. DCM (50 mL) was added and the organic layer was washed with water, brine, dried over anhydrous Na_2SO_4 and concentrated under reduced pressure. The crude product was purified by flash chromatography eluted with 5-10% v/v MeOH in DCM to afford a colorless oil (47.2 mg, 81%). HPLC t_R = 4.59 min (> 95% purity [220.8 nm]). ^{1}H NMR (400 MHz, CDCl$_3$) δ 7.75 (d, J = 7.0 Hz, 2H), 7.30 (d, J = 7.9 Hz, 2H), 4.11 (t, J = 4.4 Hz, 2H), 3.67 – 3.52 (m, 76H), 3.34 (t, J = 5.1 Hz, 2H), 2.41 (s, 3H). ^{13}C NMR (101 MHz, CDCl$_3$) δ 144.79, 133.15, 129.85, 128.00, 70.77, 70.73, 70.70, 70.67, 70.60, 70.55, 70.05, 69.27, 68.71, 50.74, 21.65.

5-(3-(37-azido-2,5,8,11,14,17,20,23,26,29,32,35-dodecaoxahepta   triacontyl)-5-(3-(2-chloro-4-fluorophenoxy)azetidin-1-yl)-4H-1,2,4-triazol-4-yl)-2-methoxypyridine (7c). To a solution of **5** (19.5 mg, 47.9 µmol, 1 eq.) in anhydrous DMF (3 mL) at iced water temperature was added KOH (19 mg, 302 µmol, 6.3 eq.). The solution was stirred for 5 min before a solution of **6c** (34.8 mg, 47.9 µmol, 1 eq.) in anhydrous DMF (3 mL) was added. The mixture was stirred at iced water temperature for 1.5 h and at 25 °C for 1 h. DMF was evaporated, to the residue DCM (70 mL) was added and the organic layer was washed with water, brine, dried over anhydrous Na_2SO_4, concentrated under vacuum and lyophilized to afford a yellow oil (42,5 mg, 92%). HPLC t_R = 4.56 min (> 95% purity [220.8 nm]). ^{1}H NMR (400 MHz, CDCl$_3$) δ 8.22 (d, J = 2.7 Hz, 1H), 7.67 (dd, J = 8.9, 2.7 Hz, 1H), 7.13 (dd, J = 8.0, 3.0 Hz, 1H), 6.86 (d, J = 8.7 Hz, 2H), 6.51 (dd, J = 9.0, 4.7 Hz, 1H), 4.90 (p, J = 5.7 Hz, 1H), 4.42 (s, 2H), 4.18 – 4.10 (m, 2H), 4.05 – 4.00 (m, 2H), 3.99 (s, 3H), 3.70 – 3.53 (m, 46H), 3.38 (t, J = 5.0 Hz, 2H).^{13}C NMR (101 MHz, CDCl$_3$) δ 164.42, 158.34, 149.74, 148.88, 145.56, 137.74, 123.58, 118.26, 118.00, 114.31, 114.09, 111.78, 70.72, 70.70, 70.66, 70.59, 70.52, 70.27, 70.05, 69.30, 68.86, 62,45, 59.46, 54.09, 50.74.

5-(3-(3-((λ[1]-oxidaneyl)methyl)-59-azido-2,6,9,12,15,18,21,24,27,   30,33,36,39,42,45,48,51,54,57-nonadecaoxanonapentacontyl)-5-(3-(2-chloro-4-fluorophenoxy)azetidin-1-yl)-4H-1,2,4-triazol-4-yl)-2-methoxypyridine (7d). To a solution of **5** (10.0 mg, 24.6 µmol, 1 eq.) in anhydrous DMF (1.7 mL) at iced water temperature was added KOH (19 mg, 295 µmol, 14 eq.). The solution was stirred for 10 min before a solution of **6d** (26.6 mg, 24.6 µmol, 1 eq.) in anhydrous DMF (1.6 mL) was added. The mixture was stirred at iced water temperature for 30 min and at 25 °C for 2.5 h. DCM (70 mL) was added and the organic layer was washed with water, brine, dried over anhydrous Na_2SO_4 and concentrated under reduced pressure. The crude product was purified by semi-preparative HPLC using a linear gradient of 20-50% ACN (0.1% v/v TFA) in H_2O (0.1% v/v TFA) in 30 min to afford after lyophilization a colorless oil (23.2 mg, 72%). HPLC t_R = 4.67 min (> 95% purity [220.8 nm]). ^{1}H NMR (400 MHz, CDCl$_3$) δ 8.32 (s, 1H), 7.81 (d, J = 8.7 Hz, 1H), 7.12 (dd, J = 7.9, 2.7 Hz, 1H), 6.95 – 6.85 (m, 2H), 6.55 (dd, J = 9.2, 4.6 Hz, 1H), 4.99 (s, 1H), 4.49 (s, 2H), 4.40 (s, 2H), 4.13 (d, J = 7.4 Hz, 2H), 4.01 (s, 3H), 3.64 (s, 78H), 3.38 (t, J = 5.0 Hz, 2H). LRMS (ESI) calcd for $C_{58}H_{98}ClFN_8O_{22}$ [M+2H]$^{2+}$/2: 656.323, found: 656.283.

3-((λ[1]-oxidaneyl)methyl)-1-(5-(3-(2-chloro-4-fluorophenoxy)azetidin-1-yl)-4-(6-methoxypyridin-3-yl)-4H-1,2,4-triazol-3-yl)-2,6,9,12,15,18,21, 24,27,30,33-undecaoxapentatriacontan-35-aminium 2,2,2-trifluoroacetate (8c). Polymer-bound triphenylphosphine (70.8 mg, 3 mmol/g, 8 eq.) was added to a solution of **7c** (25.5 mg, 26.6 µmol, 1 eq.) in anhydrous THF (1 mL). The mixture was stirred under reflux for 3.5 h, then water (400 µL) was added and the obtained mixture was stirred under reflux for another 1.5 h. The mixture was filtered and the filtrate was concentrated under reduced pressure and lyophilized. The crude product was purified by semi-preparative HPLC using a linear gradient of 20-45% ACN (0.1% v/v TFA) in H_2O (0.1% v/v TFA) in 30 min to afford after lyophilization a yellow oil

(11.9 mg, 43%). HPLC t_R = 3.94 min (> 95% purity [280.8 nm]). ^{1}H NMR (400 MHz, CDCl$_3$) δ 8.27 (d, J = 2.7 Hz, 1H), 7.77 (dd, J = 8.9, 2.7 Hz, 1H), 7.68 (s, 2H), 7.12 (dd, J = 8.0, 3.1 Hz, 1H), 6.90 (d, J = 8.7 Hz, 2H), 6.53 (dd, J = 9.1, 4.7 Hz, 1H), 5.02 – 4.89 (m, 1H), 4.43 (s, 2H), 4.39 – 4.31 (m, 2H), 4.08 (dd, J = 8.7, 3.6 Hz, 2H), 4.00 (s, 3H), 3.80 (t, J = 4.9 Hz, 2H), 3.71 – 3.56 (m, 44H), 3.23 – 3.12 (m, 2H).

3-((λ^1-oxidaneyl)methyl)-1-(5-(3-(2-chloro-4-fluorophenoxy)azetidin-1-yl)-4-(6-methoxypyridin-3-yl)-4H-1,2,4-triazol-3-yl)-2,6,9,12,15,18,21,   24,27,30,33,36,39,42,45,48,51,54,57-nonadecaoxanonapentacontan-59-aminium   2,2,2-trifluoroacetate   (8d).   Polymer-bound triphenylphosphine (33.8 mg, 3 mmol/g, 10 eq.) was added to a solution of **7d** (13.3 mg, 10.1 μmol, 1 eq.) in anhydrous THF (500 μL). The mixture was refluxed for 5 h, then water (200 μL) was added and the obtained mixture was stirred under reflux for another 2 h. The mixture was filtered and the filtrate was concentrated under reduced pressure and lyophilized. The crude product was purified by semi-preparative HPLC using a linear gradient of 20-45% ACN (0.1% v/v TFA) in H$_2$O (0.1% v/v TFA) in 30 min to afford after lyophilization a colorless oil (5.8 mg, 44%). HPLC t_R = 4.32 min (> 95% purity [220.8 nm]). ^{1}H NMR (400 MHz, CDCl$_3$) δ 8.20 (d, J = 2.7 Hz, 1H), 7.65 (dd, J = 8.8, 2.7 Hz, 1H), 7.10 (dd, J = 8.0, 3.0 Hz, 1H), 6.89 – 6.77 (m, 2H), 6.49 (dd, J = 9.0, 4.7 Hz, 1H), 4.88 (p, J = 6.2, 5.6 Hz, 1H), 4.39 (s, 2H), 4.17 – 4.05 (m, 2H), 4.04 – 3.97 (m, 2H), 3.97 (s, 3H), 3.66 – 3.58 (m, 78H), 2.99 (t, J = 5.0 Hz, 2H). LRMS (ESI) calcd for C$_{58}$H$_{100}$ClFN$_6$O$_{22}$ [M+2H]$^{2+}$/2: 643.328, found: 643.764.

Pf-PEG$_4$-NR. To a solution of **4** (3.6 mg, 9.17 μmol, 1 eq.) in anhydrous DMF (300 μL) were added a solution of **8a** (7.0 mg, 10.1 μmol, 1.1 eq.) in anhydrous DMF (300 μL), a solution of PYBOP (13.6 mg, 26.3 μmol, 2.6 eq.) in anhydrous DMF (300 μL) and DIPEA (13.3 μL, 80.6 μmol, 8 eq.). The mixture was stirred at 25 °C for 1 h and the product was then isolated by semi-preparative HPLC using a linear gradient of 20-60% ACN (0.1% v/v TFA) in H$_2$O (0.1% v/v TFA) in 30 min to afford after lyophilization a dark purple solid (6.8 mg, 78 %). HPLC t_R = 5.37 min (> 95% purity [220.8 nm]). HRMS (ESI) calcd for C$_{48}$H$_{54}$ClFN$_8$O$_{10}$ [M+2H]$^{2+}$/2: 478.1818; found: 478.1824.

Pf-PEG$_8$-NR. To a solution of **4** (0.63 mg, 1.61 μmol, 1 eq.) in anhydrous DMF (65 μL) were added a solution of **8b** (1.40 mg, 1.61 μmol, 1 eq.) in anhydrous DMF (65 μL), a solution of PYBOP (2.09 mg, 4.02 μmol, 2.5 eq.) in anhydrous DMF (65 μL) and DIPEA (2.13 μL, 12.9 μmol, 8 eq.). The mixture was stirred at 25 °C for 30 min and then were added PYBOP (2.09 mg, 4.02 μmol, 2.5 eq.) and DIPEA (2.13 μL, 12.9 μmol, 8 eq.). The mixture was stirred at 25 °C for 2 h and the product was then isolated by semi-preparative HPLC using a linear gradient of 20-60% ACN (0.1% v/v TFA) in H$_2$O (0.1% v/v TFA) in 30 min to afford after lyophilization a black purple solid (1.3 mg, 71%). HPLC t_R = 5.39 min (> 95% purity [220.8 nm]). HRMS (ESI) calcd for C$_{56}$H$_{70}$ClFN$_8$O$_{14}$ [M+2H]$^{2+}$/2: 566.2342, found: 566.2341.

Pf-PEG$_{12}$-NR. To a solution of **8c** (3.40 mg, 3.25 μmol, 1.1 eq.) in anhydrous DMF (290 μL) were added **4** (1.16 mg, 2.96 μmol, 1 eq.), PYBOP (4.38 mg, 8.42 μmol, 2.6 eq.) and DIPEA (4.29 μL, 26.0 μmol, 8 eq.). The mixture was stirred at 25 °C for 30 min and the product was then isolated by semi-preparative HPLC using a linear gradient of 20-55% ACN (0.1% v/v TFA) in H$_2$O (0.1% v/v TFA) in 30 min to afford after lyophilization a dark purple solid (1.50 mg, 39%). HPLC t_R = 5.37 min (> 95% purity [220.8 nm]). HRMS (ESI) calcd for C$_{64}$H$_{86}$ClFN$_8$O$_{18}$ [M+2H]$^{2+}$/2: 654.2866, found: 654.2871.

Pf-PEG$_{20}$-NR. To a solution of **8d** (2.70 mg, 1.93 μmol, 1 eq.) in anhydrous DMF (172 μL) were added **4** (1.51 mg, 3.86 μmol, 2 eq.), PYBOP (7.53 mg, 14.5 μmol, 7 eq.) and DIPEA (10.2 μL, 61.7 μmol, 32 eq.). The mixture was stirred at 25 °C for 25 h and the product was then isolated by semi-preparative

HPLC using a linear gradient of 20-60% ACN (0.1% v/v TFA) in H_2O (0.1% v/v TFA) to afford after lyophilization a dark purple solid (1.60 mg, 50%). HPLC t_R = 5.58 min (> 95% purity [220.8 nm]). HRMS (ESI) calcd for $C_{80}H_{119}ClFN_8O_{26}$ $[M+3H]^{3+}/3$: 554.2583, found: 554.2582.

Absorption and Steady-State Fluorescence Measurements

General information. The excitation wavelength was 520 nm and the recorded emission spectral range was 530 – 800 nm. Unless specified, all fluorescence spectra were corrected for instrumental factors. The absorbance of sample solutions at the excitation wavelength were kept below 0.05 to avoid inner filter effects. Data treatment was performed using Origin software.

Determination of fluorescence quantum yields. Determination of relative fluorescence quantum yields (QY) was performed using Nile Red in 1,4-dioxane as a reference (QY = 70%).[44]

Preparation of 1 mM DOPC/cholesterol (2:1) liposomes. To a solution of DOPC (667 µL, 5 mM) in $CHCl_3$ was added a solution of cholesterol (333 µL, 5 mM) in $CHCl_3$ and the solvent was slowly evaporated under reduced pressure. The obtained film was rehydrated with PBS (5 mL, pH 7.1 - 7.5), vortexed for 5 min and kept at 25 °C for 30 min. The suspension of multilamellar vesicles was extruded by using a Lipex Biomembranes extruder using a 0.2 µm filter for 7 passages and then 0.1 µm filter for 10 passages. This generates monodisperse LUVs were characterized by a mean diameter of 0.15 µm as measured with a Malvern Zetamaster 300 particle size analyser.

Evaluation of non-specific interactions with liposomes. The 1 µM solutions of the studied probes in PBS with increasing amounts of DOPC/cholesterol (2:1) liposomes were prepared as follows. 5 µL of 0.2 mM stock DMSO solution of a studied probe were added accordingly to 995 µL, 993 µL, 991 µL, 985 µL, 975 µL, 945 µL, 895 µL and 795 µL of PBS. Then 0 µL, 2 µL, 4 µL, 10 µL, 20 µL, 50 µL, 100 µL and 200 µL of 1 mM DOPC/cholesterol (2:1) liposomes were respectively added and the solutions were carefully mixed.

Evaluation of non-specific interactions with BSA. The titrations of the studied probes with BSA were performed as follows. 1 µM solution of the studied probes in PBS were prepared by diluting 5 µL of 0.2 mM DMSO stock solutions in 995 µL of PBS. Then successively 5 µL, 5 µL, 15 µL, 25 µL, 60 µL of 0.2 mM stock solution of BSA in PBS were added and the solutions were carefully mixed.

RTG calculation for Pf-PEG$_{20}$-NR in solutions. First, the corrected fluorescence spectra were integrated from 530 to 600 nm ("green" channel) and from 600 nm to 700 nm ("red" channel). RTG was calculated as a ratio of the integral fluorescence in the "red" channel to the integral fluorescence in the "green" channel.

Functional Characterisation of the OTR ligands

Antagonist properties of the OTR ligands were determined by measuring their capacities to inhibit oxytocin-induced intracellular Ca^{2+} release. HEK293 cells stably overexpressing the OTR were first incubated with 5 µM of Indo-1 AM in HEPES buffer (10 mM HEPES, 137.5 mM NaCl, 1.25 mM $MgCl_2$, 1.25 mM $CaCl_2$, 6 mM KCl, 0.4 mM NaH_2PO_4 and 5.6 mM glucose, pH 7.4) supplemented with 0.1% BSA for 45 minutes at 37 °C and 5% CO_2. The cells were then washed, resuspended in HEPES buffer supplemented with 0.1% BSA buffer, seeded into 384 well polystyrene plates (Greiner 781091)

at 50000 cells/well and then centrifuged for 5 min at 800 rpm. Addition of compounds was performed using the FlexStation® 3 automated pipettor. Compounds were tested at concentrations from 0.3 pM to 3 µM in the presence of 10 nM of oxytocin. Intracellular Ca^{2+} release measurements were performed by monitoring the fluorescence of Indo-1 using a FlexStation® 3 microplate reader (Molecular Devices Corp.). Excitation was set at 338 nm, emissions were recorded at 401 nm and 475 nm at 25 °C. Fluorescence emission ratio 401 nm/ 475 nm was calculated in order to follow the calcium release. In order to assess the maximum calcium level, addition of digitonin (Sigma Aldrich) at 100 µM was performed 110 s after the addition of the compounds. Dose-response curves were obtained by plotting the normalized signal of calcium release against the logarithmic values of compound concentration. The half maximal inhibitory concentration (IC_{50}) were calculated using GraphPad Prism software. Data resulted from two independent experiments performed in duplicate. Values are means ± SEM.

Fluorescence Confocal Microscopy

Cell lines and culture conditions. HEK293 cells stably overexpressing the OTR were cultured in Eagle's minimal essential medium (MEM, Invitrogen 21090) with 10% FBS, 100 U/mL of penicillin, 100 µg/mL of streptomycin, 2 mM of glutamine and 500 µg/mL of G418 at 37 °C in a humidified 5% CO_2 atmosphere. 70-80% cell confluence was maintained by removal of a portion of the culture and replacement with fresh medium twice a week. Cells were seeded into 35 mm ibiTreat µ-dish (IBiDi) at 40 000 cells per dish 3 days before imaging.

Live-cell no-wash OTR imaging. The culture medium was removed, the cells were washed with PBS and incubated with a 1 µg/mL solution of Hoechst 33342 in MEM for 15 min at 37 °C. The medium was removed, the cells were washed with PBS and a 10 nM solution of the studied probe in PBS or a mixture of 10 nM of the studied probe and 2 µM of carbetocin in PBS were added. The cells were incubated for 20 min at 37 °C prior to the imaging. The imaging was performed at 22 °C. Nile Red was excited with a 488 nm 10 mW laser at 80% intensity and detected at 570 - 630 nm. Hoechst 33342 was excited with a 405 nm 25 mW laser at 10% intensity and detected at 430 - 480 nm. The pinhole was set to 1 airy unit. The images were acquired at 1.5x magnification as a mean of 2 scans in 1024x1024 size. All images were processed with ImageJ. An additional 2x magnification was applied upon processing. The same brightness and contrast parameters for the Nile Red channel were applied to all the images.

MβCD treatments. The culture medium was removed, the cells were washed with Opti-MEM (no phenol red) and incubated with a freshly prepared 5 mM solution of MβCD in Opti-MEM (no phenol red) for 30 min at 37 °C. The cells were then washed with Opti-MEM (no phenol red) and incubated with corresponding probes.

Ratiometric confocal microscopy imaging. The culture medium was removed, the cells were washed with Opti-MEM (no phenol red) and incubated with 20 nM solutions of the studied probes in Opti-MEM (no phenol red) for 20 min at 37 °C. The imaging was performed at 22 °C. Nile Red was excited with a 488 nm 10 mW laser at 30% (Pf-PEG$_4$-NR), 50% (Pf-PEG$_8$-NR) or 80% (for other probes). The fluorescence was collected from 500 nm to 600 nm ("green" channel C1) and from 600 nm to 700 nm ("red" channel C2). Images were acquired at 1.5x magnification in 512x512 size, 20 scans in each channel. All images were processed with ImageJ. Fluorescence intensity in each channel was averaged using z-stack projection. The mean of grey values of background signal was subtracted in both channels. Membrane ROI were created using the "Otsu" threshold. RTG values of the cell membrane were calculated by dividing the mean of grey values in the obtained masks in C2 by that in C1. The ratiometric

confocal microscopy images were generated using the ImageJ macros "Ratio Intensity color Version 2.5" (developed by Romain Vauchelles, UMR 7213) that divides background-subtracted image of the "red" channel bybackground-subtracted image of the "green" channel. For each pixel, a pseudocolor scale is used for coding the RTG ratio.

Keywords: fluorescent probes • fluorogenic dyes • turn-on probes • cell imaging • GPCR

References

(1)   Hauser, A. S.; Attwood, M. M.; Rask-Andersen, M.; Schiöth, H. B.; Gloriam, D. E. Trends in GPCR Drug Discovery: New Agents, Targets and Indications. *Nat Rev Drug Discov* **2017**, *16* (12), 829–842. https://doi.org/10.1038/nrd.2017.178.

(2)   Santos, R.; Ursu, O.; Gaulton, A.; Bento, A. P.; Donadi, R. S.; Bologa, C. G.; Karlsson, A.; Al-Lazikani, B.; Hersey, A.; Oprea, T. I.; Overington, J. P. A Comprehensive Map of Molecular Drug Targets. *Nat Rev Drug Discov* **2017**, *16* (1), 19–34. https://doi.org/10.1038/nrd.2016.230.

(3)   Davenport, A. P.; Scully, C. C. G.; de Graaf, C.; Brown, A. J. H.; Maguire, J. J. Advances in Therapeutic Peptides Targeting G Protein-Coupled Receptors. *Nat Rev Drug Discov* **2020**, *19* (6), 389–413. https://doi.org/10.1038/s41573-020-0062-z.

(4)   Sriram, K.; Insel, P. A. G Protein-Coupled Receptors as Targets for Approved Drugs: How Many Targets and How Many Drugs? *Mol Pharmacol* **2018**, *93* (4), 251–258. https://doi.org/10.1124/mol.117.111062.

(5)   Hilger, D.; Masureel, M.; Kobilka, B. K. Structure and Dynamics of GPCR Signaling Complexes. *Nat Struct Mol Biol* **2018**, *25* (1), 4–12. https://doi.org/10.1038/s41594-017-0011-7.

(6)   Weis, W. I.; Kobilka, B. K. The Molecular Basis of G Protein–Coupled Receptor Activation. *Annu. Rev. Biochem.* **2018**, *87* (1), 897–919. https://doi.org/10.1146/annurev-biochem-060614-033910.

(7)   Congreve, M.; de Graaf, C.; Swain, N. A.; Tate, C. G. Impact of GPCR Structures on Drug Discovery. *Cell* **2020**, *181* (1), 81–91. https://doi.org/10.1016/j.cell.2020.03.003.

(8)   Lingwood, D.; Simons, K. Lipid Rafts As a Membrane-Organizing Principle. *Science* **2010**, *327* (5961), 46–50. https://doi.org/10.1126/science.1174621.

(9)   Sezgin, E.; Levental, I.; Mayor, S.; Eggeling, C. The Mystery of Membrane Organization: Composition, Regulation and Roles of Lipid Rafts. *Nat Rev Mol Cell Biol* **2017**, *18* (6), 361–374. https://doi.org/10.1038/nrm.2017.16.

(10)   Wiseman, D. N.; Otchere, A.; Patel, J. H.; Uddin, R.; Pollock, N. L.; Routledge, S. J.; Rothnie, A. J.; Slack, C.; Poyner, D. R.; Bill, R. M.; Goddard, A. D. Expression and Purification of Recombinant G Protein-Coupled Receptors: A Review. *Protein Expression and Purification* **2020**, *167*, 105524. https://doi.org/10.1016/j.pep.2019.105524.

(11)   Wacker, D.; Stevens, R. C.; Roth, B. L. How Ligands Illuminate GPCR Molecular Pharmacology. *Cell* **2017**, *170* (3), 414–427. https://doi.org/10.1016/j.cell.2017.07.009.

(12)   Huber, T.; Sakmar, T. P. Chemical Biology Methods for Investigating G Protein-Coupled Receptor Signaling. *Chemistry & Biology* **2014**, *21* (9), 1224–1237. https://doi.org/10.1016/j.chembiol.2014.08.009.

(13)   Grunbeck, A.; Sakmar, T. P. Probing G Protein-Coupled Receptor—Ligand Interactions with Targeted Photoactivatable Cross-Linkers. *Biochemistry* **2013**, *52* (48), 8625–8632. https://doi.org/10.1021/bi401300y.

(14)   Ciruela, F.; Jacobson, K. A.; Fernández-Dueñas, V. Portraying G Protein-Coupled Receptors with Fluorescent Ligands. *ACS Chem. Biol.* **2014**, *9* (9), 1918–1928. https://doi.org/10.1021/cb5004042.

(15)   Ma, Z.; Du, L.; Li, M. Toward Fluorescent Probes for G-Protein-Coupled Receptors (GPCRs): Miniperspective. *J. Med. Chem.* **2014**, *57* (20), 8187–8203. https://doi.org/10.1021/jm401823z.

(16)   Soave, M.; Briddon, S. J.; Hill, S. J.; Stoddart, L. A. Fluorescent Ligands: Bringing Light to Emerging GPCR Paradigms. *Br J Pharmacol* **2020**, *177* (5), 978–991. https://doi.org/10.1111/bph.14953.

(17)   Tian, H.; Fürstenberg, A.; Huber, T. Labeling and Single-Molecule Methods To Monitor G Protein-Coupled Receptor Dynamics. *Chem. Rev.* **2017**, *117* (1), 186–245. https://doi.org/10.1021/acs.chemrev.6b00084.

(18)   Demchenko, A. P.; Mély, Y.; Duportail, G.; Klymchenko, A. S. Monitoring Biophysical Properties of Lipid Membranes by Environment-Sensitive Fluorescent Probes. *Biophysical Journal* **2009**, *96* (9), 3461–3470. https://doi.org/10.1016/j.bpj.2009.02.012.

(19)   Klymchenko, A. S. Solvatochromic and Fluorogenic Dyes as Environment-Sensitive Probes: Design and Biological Applications. *Acc. Chem. Res.* **2017**, *50* (2), 366–375. https://doi.org/10.1021/acs.accounts.6b00517.

(20)   Dijkman, P. M.; Watts, A. Lipid Modulation of Early G Protein-Coupled Receptor Signalling Events. *Biochimica et Biophysica Acta (BBA) - Biomembranes* **2015**, *1848* (11), 2889–2897. https://doi.org/10.1016/j.bbamem.2015.08.004.

(21)   Mondal, S.; Khelashvili, G.; Johner, N.; Weinstein, H. How the Dynamic Properties and Functional Mechanisms of GPCRs Are Modulated by Their Coupling to the Membrane Environment. In *G Protein-Coupled Receptors - Modeling and Simulation*; Filizola, M., Ed.; Advances in Experimental Medicine and Biology; Springer Netherlands: Dordrecht, 2014; Vol. 796, pp 55–74. https://doi.org/10.1007/978-94-007-7423-0_4.

(22)   Gahbauer, S.; Böckmann, R. A. Comprehensive Characterization of Lipid-Guided G Protein-Coupled Receptor Dimerization. *J. Phys. Chem. B* **2020**, *124* (14), 2823–2834. https://doi.org/10.1021/acs.jpcb.0c00062.

(23)   Gahbauer, S.; Böckmann, R. A. Membrane-Mediated Oligomerization of G Protein Coupled Receptors and Its Implications for GPCR Function. *Front. Physiol.* **2016**, *7*. https://doi.org/10.3389/fphys.2016.00494.

(24)   Bolivar, J. H.; Muñoz-García, J. C.; Castro-Dopico, T.; Dijkman, P. M.; Stansfeld, P. J.; Watts, A. Interaction of Lipids with the Neurotensin Receptor 1. *Biochimica et Biophysica Acta (BBA) - Biomembranes* **2016**, *1858* (6), 1278–1287. https://doi.org/10.1016/j.bbamem.2016.02.032.

(25)   Yoshida, K.; Nagatoishi, S.; Kuroda, D.; Suzuki, N.; Murata, T.; Tsumoto, K. Phospholipid Membrane Fluidity Alters Ligand Binding Activity of a G Protein-Coupled Receptor by Shifting the Conformational Equilibrium. *Biochemistry* **2019**, *58* (6), 504–508. https://doi.org/10.1021/acs.biochem.8b01194.

(26)   Becher, A.; McIlhinney, R. A. J. Consequences of Lipid Raft Association on G-Protein-Coupled Receptor Function. *Biochemical Society Symposia* **2005**, *72*, 151–164. https://doi.org/10.1042/bss0720151.

(27)   Levental, I.; Levental, K. R.; Heberle, F. A. Lipid Rafts: Controversies Resolved, Mysteries Remain. *Trends in Cell Biology* **2020**, *30* (5), 341–353. https://doi.org/10.1016/j.tcb.2020.01.009.

(28)   Dietrich, C.; Bagatolli, L. A.; Volovyk, Z. N.; Thompson, N. L.; Levi, M.; Jacobson, K.; Gratton, E. Lipid Rafts Reconstituted in Model Membranes. *Biophysical Journal* **2001**, *80* (3), 1417–1428. https://doi.org/10.1016/S0006-3495(01)76114-0.

(29)   Jin, L.; Millard, A. C.; Wuskell, J. P.; Dong, X.; Wu, D.; Clark, H. A.; Loew, L. M. Characterization and Application of a New Optical Probe for Membrane Lipid Domains. *Biophysical Journal* **2006**, *90* (7), 2563–2575. https://doi.org/10.1529/biophysj.105.072884.

(30)   Kucherak, O. A.; Oncul, S.; Darwich, Z.; Yushchenko, D. A.; Arntz, Y.; Didier, P.; Mély, Y.; Klymchenko, A. S. Switchable Nile Red-Based Probe for Cholesterol and Lipid Order at the Outer Leaflet of Biomembranes. *J. Am. Chem. Soc.* **2010**, *132* (13), 4907–4916. https://doi.org/10.1021/ja100351w.

(31)   Danylchuk, D. I.; Moon, S.; Xu, K.; Klymchenko, A. S. Switchable Solvatochromic Probes for Live-Cell Super-resolution Imaging of Plasma Membrane Organization. *Angew. Chem. Int. Ed.* **2019**, *58* (42), 14920–14924. https://doi.org/10.1002/anie.201907690.

(32)   Klymchenko, A. S.; Kreder, R. Fluorescent Probes for Lipid Rafts: From Model Membranes to Living Cells. *Chemistry & Biology* **2014**, *21* (1), 97–113. https://doi.org/10.1016/j.chembiol.2013.11.009.

(33)   Buenaventura, T.; Bitsi, S.; Laughlin, W. E.; Burgoyne, T.; Lyu, Z.; Oqua, A. I.; Norman, H.; McGlone, E. R.; Klymchenko, A. S.; Corrêa, I. R.; Walker, A.; Inoue, A.; Hanyaloglu, A.; Grimes, J.; Koszegi, Z.; Calebiro, D.; Rutter, G. A.; Bloom, S. R.; Jones, B.; Tomas, A. Agonist-Induced Membrane Nanodomain Clustering Drives GLP-1 Receptor Responses in Pancreatic Beta Cells. *PLoS Biol* **2019**, *17* (8), e3000097. https://doi.org/10.1371/journal.pbio.3000097.

(34)   Karpenko, I. A.; Kreder, R.; Valencia, C.; Villa, P.; Mendre, C.; Mouillac, B.; Mély, Y.; Hibert, M.; Bonnet, D.; Klymchenko, A. S. Red Fluorescent Turn-On Ligands for Imaging and Quantifying G Protein-Coupled Receptors in Living Cells. *ChemBioChem* **2014**, *15* (3), 359–363. https://doi.org/10.1002/cbic.201300738.

(35)   Darwich, Z.; Klymchenko, A. S.; Dujardin, D.; Mély, Y. Imaging Lipid Order Changes in Endosome Membranes of Live Cells by Using a Nile Red-Based Membrane Probe. *RSC Adv.* **2014**, *4* (17), 8481–8488. https://doi.org/10.1039/C3RA47181K.

(36)   Kreder, R.; Pyrshev, K. A.; Darwich, Z.; Kucherak, O. A.; Mély, Y.; Klymchenko, A. S. Solvatochromic Nile Red Probes with FRET Quencher Reveal Lipid Order Heterogeneity in Living and Apoptotic Cells. *ACS Chem. Biol.* **2015**, *10* (6), 1435–1442. https://doi.org/10.1021/cb500922m.

(37)   Brown, A.; Brown, T. B.; Calabrese, A.; Ellis, D.; Puhalo, N.; Ralph, M.; Watson, L. Triazole Oxytocin Antagonists: Identification of an Aryloxyazetidine Replacement for a Biaryl Substituent. *Bioorganic & Medicinal Chemistry Letters* **2010**, *20* (2), 516–520. https://doi.org/10.1016/j.bmcl.2009.11.097.

(38)   Karpenko, I. A.; Margathe, J.-F.; Rodriguez, T.; Pflimlin, E.; Dupuis, E.; Hibert, M.; Durroux, T.; Bonnet, D. Selective Nonpeptidic Fluorescent Ligands for Oxytocin Receptor: Design, Synthesis, and Application to Time-Resolved FRET Binding Assay. *J. Med. Chem.* **2015**, *58* (5), 2547–2552. https://doi.org/10.1021/jm501395b.

(39)   Briggs, M. S. J.; Bruce, I.; Miller, J. N.; Moody, C. J.; Simmonds, A. C.; Swann, E. Synthesis of Functionalised Fluorescent Dyes and Their Coupling to Amines and Amino Acids. *J. Chem. Soc., Perkin Trans. 1* **1997**, No. 7, 1051–1058. https://doi.org/10.1039/a605012c.

(40)   Martin-Brown, S. A.; Fu, Y.; Saroja, G.; Collinson, M. M.; Higgins, D. A. Single-Molecule Studies of Diffusion by Oligomer-Bound Dyes in Organically Modified Sol–Gel-Derived Silicate Films. *Anal. Chem.* **2005**, *77* (2), 486–494. https://doi.org/10.1021/ac0491511.

(41)   Kashida, H.; Asanuma, H. Preparation of Supramolecular Chromophoric Assemblies Using a DNA Duplex. *Phys. Chem. Chem. Phys.* **2012**, *14* (20), 7196. https://doi.org/10.1039/c2cp40520b.

(42) Mukherjee, S.; Raghuraman, H.; Chattopadhyay, A. Membrane Localization and Dynamics of Nile Red: Effect of Cholesterol. *Biochimica et Biophysica Acta (BBA) - Biomembranes* **2007**, *1768* (1), 59–66. https://doi.org/10.1016/j.bbamem.2006.07.010.

(43) Greenspan, P.; Mayer, E. P.; Fowler, S. D. Nile Red: A Selective Fluorescent Stain for Intracellular Lipid Droplets. *The Journal of Cell Biology* **1985**, *100* (3), 965–973. https://doi.org/10.1083/jcb.100.3.965.

(44) Sackett, D. L.; Wolff, J. Nile Red as a Polarity-Sensitive Fluorescent Probe of Hydrophobic Protein Surfaces. *Analytical Biochemistry* **1987**, *167* (2), 228–234. https://doi.org/10.1016/0003-2697(87)90157-6.

(45) Lampe, J. N.; Fernandez, C.; Nath, A.; Atkins, W. M. Nile Red Is a Fluorescent Allosteric Substrate of Cytochrome P450 3A4 [†]. *Biochemistry* **2008**, *47* (2), 509–516. https://doi.org/10.1021/bi7013807.

(46) Black, S. L.; Stanley, W. A.; Filipp, F. V.; Bhairo, M.; Verma, A.; Wichmann, O.; Sattler, M.; Wilmanns, M.; Schultz, C. Probing Lipid- and Drug-Binding Domains with Fluorescent Dyes. *Bioorganic & Medicinal Chemistry* **2008**, *16* (3), 1162–1173. https://doi.org/10.1016/j.bmc.2007.10.080.

(47) Ashoka, A. H.; Ashokkumar, P.; Kovtun, Y. P.; Klymchenko, A. S. Solvatochromic Near-Infrared Probe for Polarity Mapping of Biomembranes and Lipid Droplets in Cells under Stress. *J. Phys. Chem. Lett.* **2019**, *10* (10), 2414–2421. https://doi.org/10.1021/acs.jpclett.9b00668.

(48) Waltenspühl, Y.; Schöppe, J.; Ehrenmann, J.; Kummer, L.; Plückthun, A. Crystal Structure of the Human Oxytocin Receptor. *Sci. Adv.* **2020**, *6* (29), eabb5419. https://doi.org/10.1126/sciadv.abb5419.

(49) Mahammad, S.; Parmryd, I. Cholesterol Depletion Using Methyl-β-Cyclodextrin. In *Methods in Membrane Lipids*; Owen, D. M., Ed.; Springer New York: New York, NY, 2015; Vol. 1232, pp 91–102. https://doi.org/10.1007/978-1-4939-1752-5_8.

(50) Zhang, P.; Lindsay, S.; Manna, S.; Senapati, S. Linker Molecule for Multiplex Recognition by Atomic Force Microscopy (AFM). US 2017/0137389 Al, May 18, 2017.